

Article

State of Charge Control Integrated with Load Frequency Control for BESS in Islanded Microgrid

Sandro Sitompul ^{1,*} , Yuki Hanawa ¹, Verapatra Bupphaves ² and Goro Fujita ¹

¹ Department of Electrical and Electronics Engineering, Shibaura Institute of Technology, 3-7-5 Toyosu, Tokyo 135-8548, Japan; ae16068@shibaura-it.ac.jp (Y.H.); gfujita@sic.shibaura-it.ac.jp (G.F.)

² Nippon Koei Co., Ltd., 4-2 Kojimachi, Tokyo 102-8539, Japan; a8713@n-koei.co.jp

* Correspondence: na18502@shibaura-it.ac.jp

Received: 24 June 2020; Accepted: 1 September 2020; Published: 8 September 2020



Abstract: The dependence of distributed generations (DGs) on climate conditions and fluctuating load demands are the challenges for the implementation of battery energy storage systems (BESSs) in islanded microgrids. BESS participation in system frequency regulation becomes one of the solutions to those challenges. Frequency regulation by BESS can be realized by applying the load-frequency control (LFC) in BESS. However, this participation clearly poses problems for the battery state of charge (SOC), as the battery is often overcharged or undercharged. In this paper, a control that maintains SOC at a certain level is introduced. This control strategy focuses on the battery operation function, which is determined from five control scenarios. All scenarios are achieved by applying the droop reference shifting method in the LFC to allow battery operation change. Control verification is carried out on an islanded microgrid system that experiences load demand changes and photovoltaic (PV) output power changes. The test results show that the SOC is maintained at 45–75% by applying load and PV power variations. The results correspond to the predetermined criteria control.

Keywords: islanded microgrid; battery energy storage system; load frequency control; state of charge

1. Introduction

In recent years, environmental issues have required the availability of clean and economically affordable energy. This causes vertically power system restructuring and has significant impacts on the electricity industry [1]. One of those changes is the widespread use of distributed generation (DG). The use of DG is increasingly widespread due to the ability to create hybrid electric systems (HES) supporting the creation of clean and economically affordable energy [2]. HES consist of several DGs, consumer, and energy storage units. Such systems are often called microgrids which can operate physically islanded or interconnected with the utility grids [3].

DG sources such as photovoltaic arrays (PV), wind turbines (WT), and fuel cells have a great influence on the system. However, the increased use of DG that lacks inertia gradually shifts the role of synchronous generator which has an impact on the reduction in system inertia. For grid-connected/interconnected microgrid, clearly this is not an issue because the frequency and voltage of the microgrid are controlled directly from the utility grid. It certainly confirms the system inertia is not an issue. On the other hand, an islanded microgrid system depends on the system inertia for its stability, and so system stability problems are often encountered when changes in the system operation occur. Frequency stability problems occur on islanded microgrid systems when power imbalances occur. This requires the availability of a fast frequency response, to resolve the stability problem [3–6]; the inability of the system to perform the response could increase severe problems in the operation and control of the islanded microgrid.

Several frequency stability issues related to islanded microgrid systems have been discussed. The reduction in inertia increases frequency oscillations of the system, as discussed in [7–14]. A frequency control strategy based on dynamically high-power machines to reduce the load is proposed in [9]. Li et al. discuss a control strategy of a virtual synchronous generator (VSG) by utilizing a self-adaptive damping control strategy [10]. In addition, a decentralized control synthesis procedure for stabilizing the frequency that enables plug-and-play (PnP) operations is introduced in [11]. The frequency-reactive control is proposed in [12–14].

One solution to the frequency problem that has adequate advantages is the battery energy storage system (BESS). The BESS has PROVEN to have the ability to provide primary frequency reserves in emergency situations. Short-term power quality and long-term energy management can be solved by BESS, which is comprised of static elements and has a fast-dynamic response compared to typical generators or other energy storage devices. The BESS demonstration shows the BESS frequency control function on the islanded system [4]. Besides, the BESS frequency control function is used on a small electric power system [1]. In many discussions, the control is referred to as load-frequency control (LFC). LFC is a control-based droop which allows the source units to regulate their output power according to the system frequency to within prescribed value.

Reference [15] introduces a primary frequency regulation using droop-based LFC installed on a grid-connected lithium-ion BESS. In [16], a study of specific control algorithms that calculate the droop and SOC management for BESS is carried out as well as a simulation of the frequency signal effects of the control. An implemented LFC at BESS using a droop that has a power limitation study is carried out. This study analyzes an index to CALCULATE BESS performance when using these controls. SOC-based droop control based on multi-agent systems (MAS) is proposed in [17]. This study shows the effect of control droop on BESS on system performance. Furthermore, the impact of communication time delay on the improved method for balancing SOC is investigated.

Most of the studies have not suggested any means of managing the battery state-of-charge (SOC). Managing the battery SOC is a critical challenge besides the battery participation in the system. The SOC feedback method for battery droop control in the frequency domain is discussed in [18]. The main tenet of this control is its ability to coordinate the role between the BESS and the generator. In [17–20], the SOC control is proposed, while maintaining the SOC at a predetermined value. This keeps the SOC at the predetermined value; however, there has been no discussion about the SOC control which still maintains the system frequency in a certain range where the SOC fluctuations affect the output of the BESS.

In a BESS application on an islanded microgrid, the BESS is operated following the load demand so the power balance will always be satisfied. However, due to the continuous participation, such an operation implies a larger BESS capacity as it is economically unattractive. Given the large operating margin of the islanded microgrid, varying the BESS output power to maintain the SOC is possible. SOC, which is managed within a certain range, will lead to a smaller capacity of the BESS installed in the system. Thus, it is necessary to have SOC control in a BESS in an islanded microgrid.

In this paper, a SOC control in which the battery output varies according to the SOC level is proposed. Variation of the output power is possible using the droop reference shift method of the proposed control. By applying the LFC and the proposed SOC control, the BESS continuously varies its output power while maintaining system stability.

2. Frequency Response of Microgrid

In an islanded microgrid system operation, the system frequency may change due to the low inertia of the installed sources. In IEEE Std. 1647.4-2011, regarding the operation of distributed resource island systems, the islanded microgrid systems are allowed to operate its frequency outside of the nominal value [21]. A variation in frequency value may occur as a result of the primary control in the microgrid control system. One of the primary controls that is often used is a droop control [9]. The droop control strategy is appropriate for systems that adopt multiple microsources that participate

in the system frequency regulation. In operation, changes in the microgrid frequency that experience disturbances or changes in the load can be written as [4]:

$$\frac{df}{dt} = \frac{f_0}{2\sum_i H_i} \left(\sum_i P_{G_i} - \sum_i P_{L_i} \right) \quad (1)$$

where $\sum_i H_i$ is the sum of the inertia constants of all rotating machines, f_0 is the nominal frequency, P_{G_i} is the inertia generator output power, and P_{L_i} is the load demand.

The rate of changes of frequency (df/dt) can be reduced by implementing some inertias due to its fundamental role. With the increase of non-inertia sources, the system inertia will also reduce due to their connection to the grid via the power electronics interface [22]. Therefore, the conventional governors owned by inertia sources may unsuccessfully compensate for the power imbalances that occurred.

In this paper, a diesel generator is applied as the inertia source. Modeled in a simple first-order at the engine output, the engine model describes the level of fuel consumption in a function of speed and mechanical power. The model connects fuel consumption with engine mechanical power. A generator has a governor system whose engine speed is controlled automatically by connecting the fuel intake. The system, which is defined as a mechanical or electromechanical device, has several types in its implementation, such as mechanical-hydraulic direct mechanical, electrohydraulic, and microprocessor-based governor. Figure 1 illustrates the governor model used in this study. By implementing droop control, the change in engine output power is directly proportional to the droop frequency. The physical unit for R which is the physical significance of the regulator feedback parameter is Hz/kW and is considered always positive [23].

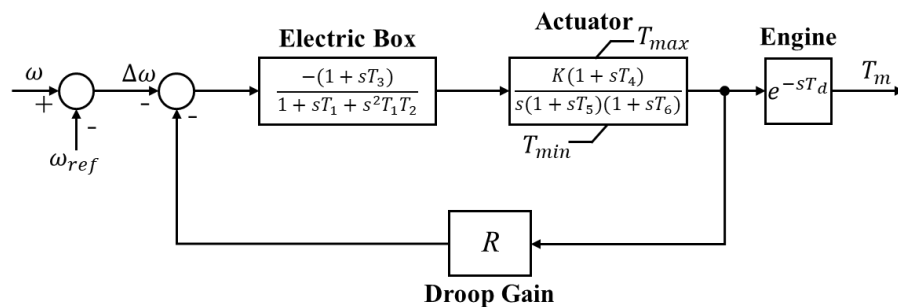


Figure 1. Diesel generator governor model.

The author [24] develops a computer model of a diesel generator that acts as an emergency generator. However, this model only applies when the system works at a fixed frequency value. Conversely, the governor model that will be used on this system is the governor model which allows the frequency value to vary (droop control). Therefore, the governor model used is the governor model developed from a model [24] which is the DEGOV1 model from [25]. Both models are modeling governor systems adapted from well-known Woodward diesel governors [26]. The difference between those two is that the model in [24] functions to maintain the frequency at its nominal value, while the DEGOV 1 model functions to variate the frequency based on the R value.

The DEGOV1 model used in this system is shown in Figure 1. It is employed to simulate torque produced by the diesel engine based on the speed signal from the governor. This model consists of an electric control box, an actuator, and a diesel engine in which all the used parameters are stated in [25].

3. BESS Model

BESS is a system containing the battery, the power conditioning system (PCS), and other components, such as the protection system for the battery and PCS. Both the battery and PCS are major components of BESS and now experiencing rapid development [27].

The battery is an arrangement of cells that can convert chemical energy into electricity and vice versa. Until now, many battery technologies have been developed where each technology has its advantages. Some of them are lead-acid, lithium-ion (Li-ion), sodium-sulfur (NaS), vanadium redox (VRB), and zinc-bromine (ZnBr). In electric power applications, lead-acid batteries are widely used because of their mature technology and the oldest among other technologies [27].

The batteries are rated in terms of energy and power capacities. For most of the battery types, the power and energy capacities are not independent. In BESS operation, several distinctive features need to be known, such as SOC, life span, efficiency, operating temperature, self-discharge, and energy density. PCS plays an essential role in BESS as an interface between the battery and the grid. Moreover, it regulates the battery charge-discharge, charging rate, etc. PCS itself is designed to allow the BESS having many functions in power system application [14,24–26].

In modeling the BESS, several essential things need to be acknowledged in SOC calculation such as PCS efficiency and output power limitation. The energy stored in the storage device is expressed as follows [20,28–30]. On charging mode ($P_b(t) < 0$), the power limitation and SOC calculation are written as:

$$-\eta P_b(t)\Delta t \leq K_C C_{bat} \quad (2)$$

$$SOC(t+1) = SOC(t) - \eta P_b(t)\Delta t \quad (3)$$

on the contrary, the power limitation and the SOC calculation when the BESS is in discharging mode ($P_b(t) > 0$) are respectively expressed as:

$$\frac{P_b(t)\Delta t}{\eta} \leq K_C C_{bat} \quad (4)$$

$$SOC(t+1) = SOC(t) - \frac{P_b(t)\Delta t}{\eta} \quad (5)$$

where η is the BESS efficiency, K_C is the maximum portion of the rated capacity that can be added and released in an hour which determines the relation between the battery power and energy, C_{bat} is the rated maximum stored energy, and Δt is the scheduling interval used in the study [30].

In a droop-based LFC, the output power of generator is proportional to the system frequency. Without any changes in the control, the generator will continue to supply power according to the predetermined ratio. However, the droop curve shift can create changes in the generator output power [12]. On the other hand, the BESS output power determines the SOC BESS at one time. For the SOC to be maintained within a predetermined range, BESS must be able to change its output power. Therefore, by applying a droop-based LFC to the BESS, droop shifting allows the BESS to change its output power while operating thus, allowing the SOC BESS to remain at the desired limits.

In this section, the integrated SOC control with the LFC is introduced. This control will allow BESS output power changes based on the SOC value. It can be achieved since the SOC information is translated by the SOC control into a frequency shift for the LFC. The shift in frequency on the droop based LFC creates a change in the output power of BESS.

This section is divided into two parts, the LFC and the SOC control. The LFC part describes multiple region active power-frequency control that defines BESS operation. In the SOC control section, the proposed control that implements a droop reference shift is introduced. Furthermore, the effect of the frequency shift on the BESS power is included in this part.

3.1. Load Frequency Control

LFC is the control of active power and frequency that is designed to suppress the power deviation and frequency deviation within a specified range [31]. The proposed LFC as the primary control configures the output of $P-f$ characteristics into multi-region curves shown in Figure 2. It allows the frequency to vary between f_{max} and f_{min} as the maximum and minimum values, f_0 is the nominal value

of the system shown in the vertical axis. On the horizontal axis, P_{bmax} and $-P_{bmax}$ show the battery maximum output power.

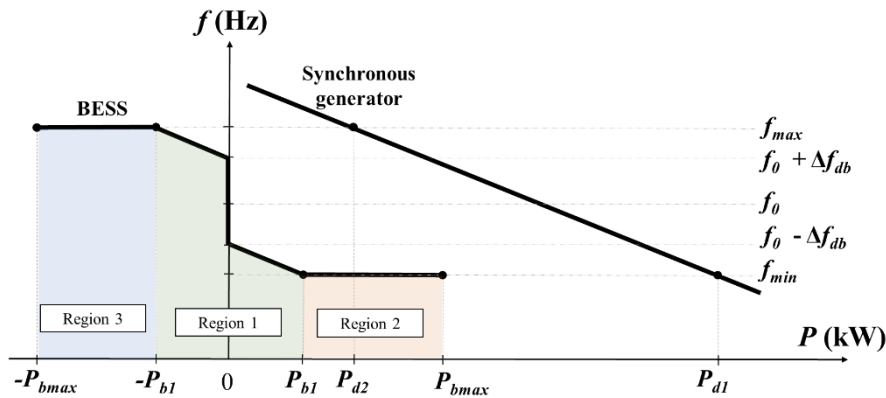


Figure 2. Battery energy storage system (BESS) multi-region load-frequency control (LFC) with generator droop.

The control is separated into three regions named Region 1, Region 2, and Region 3 that each of the regions determines the BESS operation. In Region 1, the BESS acts according to the droop curve for both charging and discharging modes with a deadband area applied to it. The deadband area allows the BESS to enter a standby mode (inactive) that will not charge or discharge its energy. In Region 2 and Region 3, the flat regions, the BESS supplies power according to the flat line while the frequency maintains at f_{max} and f_{min} . Those regions allow the synchronous generator to supply either P_{d1} (Region 2) or P_{d2} (Region 3). When the BESS operates in Region 2, the frequency is maintained at f_{min} . It puts the BESS power varies from P_{b1} to P_{bmax} and the synchronous generator supplies P_{d1} . Conversely, in Region 3, the frequency is maintained at f_{max} . It puts the BESS power varies from $-P_{b1}$ to $-P_{bmax}$ while the generator supplies P_{d2} .

3.1.1. Region 1 (Droop Control with Deadband)

In Region 1, the droop control is applied to BESS. This control allows the BESS supplying and absorbing power according to the droop equation that is expressed in (6) [32]:

$$f - f_0 = K_C(P_b - P_{b0}) \quad (6)$$

where f is the system frequency, f_0 is the nominal frequency that acts as droop reference, K_b is the BESS droop gain, P_b is the BESS output power, and P_{b0} is the BESS power at nominal frequency. In this region, a deadband area (Δf_{db}) is introduced shown in Figure 2. The BESS starts operating when the system frequency is higher than $f_0 + \Delta f_{db}$ or lower than $f_0 - \Delta f_{db}$. Apart from that, the BESS will operate in standby mode. Thus, the new droop control is written as:

$$f - (f_0 \pm \Delta f_{db}) = K_b(P_b - P_{b0}) \quad (7)$$

which the deadband area is included in the droop curve shown in Figure 2. There are two possibilities in Equation (7). When the BESS turns into charging mode, the nominal frequency that acts as droop reference will deviate into $f_0 + \Delta f_{db}$. On the other hand, the droop reference will deviate into $f_0 - \Delta f_{db}$ when the BESS turns into discharging mode.

3.1.2. Region 2 (Battery Discharging Mode Flat Frequency)

In Region 2, the BESS regulates their output power at flat frequency f_{min} shown in Figure 2. The BESS regulates its output power from P_{b1} to P_{bmax} while the generator maintains its output power

at P_{d1} . Since the frequency value comes from the generator droop curve, the frequency will follow the generator output power. Thus, the BESS power equation is expressed as:

$$f - f_{\min} = \left\{ K_b \left(K_p + \frac{K_i}{s} \right) \right\} (P_b - P_{b0}) \quad (8)$$

where K_p and K_i respectively are proportional and integration gain for the BESS control.

3.1.3. Region 3 (Battery Charging Mode Flat Frequency)

In Region 3, similar to Region 2, the BESS regulates its output power at flat frequency f_{\max} . The BESS regulates its power from $-P_{b1}$ to $-P_{b\max}$ while the generator maintains its output power at P_{d2} . Hence, the equation is expressed as:

$$f - f_{\max} = \left\{ K_b \left(K_p + \frac{K_i}{s} \right) \right\} (P_b - P_{b0}) \quad (9)$$

where K_p and K_i respectively are proportional and integration gain for the BESS control.

3.1.4. LFC Regions

Previously all the operation regions that describe their operation have been discussed. By combining all the LFC regions, the BESS power P_b is determined based on the frequency value that is written as:

$$P_b = \begin{cases} \frac{f - f_{\max}}{\left\{ K_b \left(K_p + \frac{K_i}{s} \right) \right\}} + P_{b0}; & f \geq f_{\max} \\ \frac{f - (f_0 + \Delta f_{db})}{K_b} + P_{b0}; & f_0 + \Delta f_{db} \leq f < f_{\max} \\ 0; & f_0 - \Delta f_{db} < f < f_0 + \Delta f_{db} \\ \frac{f - (f_0 - \Delta f_{db})}{K_b} + P_{b0} & f_{\min} < f \leq f_0 - \Delta f_{db} \\ \frac{f - f_{\min}}{\left\{ K_b \left(K_p + \frac{K_i}{s} \right) \right\}} + P_{b0} & f \leq f_{\min} \end{cases} \quad (10)$$

Equation (10) shows that the BESS power i calculated based on the system frequency. At the deadband area, the BESS is at standby mode ($P_b = 0$). At the droop area ($f_{\min} < f \leq f_0 - \Delta f_{db}$ or $f_0 + \Delta f_{db} \leq f < f_{\max}$), the BESS adjusts its power according to the load-sharing between the generator and BESS. When the system operates at Region 2 or Region 3 ($f \leq f_{\min}$ or $f \geq f_{\max}$), the PI droop control is performed that makes BESS regulates its power to maintain the generator power at P_{d1} or P_{d2} . Equation (10) can be represented in a block diagram control shown in Figure 3. The block diagram is divided into three parts (upper, middle, and lower). The upper part describes the Region 1 control consisting the droop control with deadband area, the middle part describes the Region 2 control consisting of the PI droop control for f_{\min} , and the lower part describes the Region 3 control consisting of the PI droop control for f_{\max} .

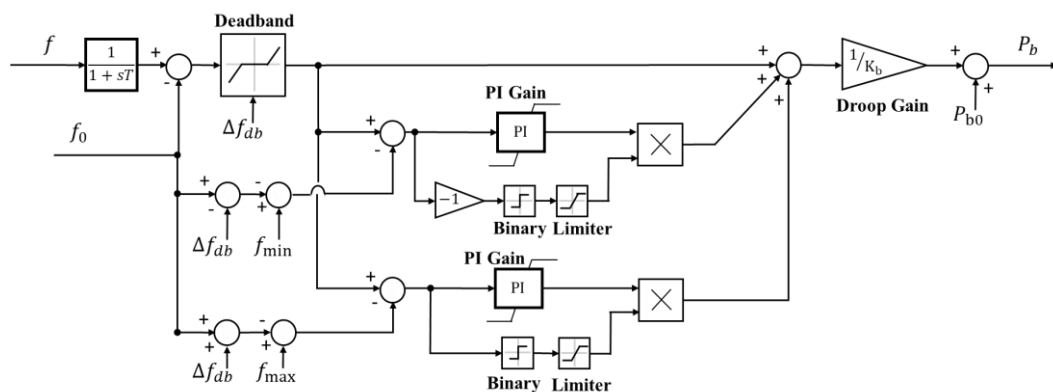


Figure 3. BESS LFC block diagram.

3.2. State-of-Charge (SOC) Control

Islanded microgrids share the same issue with stand-alone systems, namely satisfying the load balance and regulate the system microgrid voltage and frequency. In both cases, the control strategy should consider the SOC limits and the battery capacity [33]. A SOC control strategy which determines the BESS operation for each region is discussed in this subsection.

The proposed SOC control strategy is shown in Figure 4. This strategy is divided into five control scenarios according to the SOC condition. These scenarios are upper critical state (UCS), upper limit (UL), power sharing (PS), lower limit (LL), and lower critical state (LCS). The proposed strategy can be performed by implementing a shifting droop control as the battery SOC control. The BESS LFC with the SOC control effect is shown by the colored lines in Figure 5. Thus, by applying the droop Equation (7), the colored curve shift can be expressed as:

$$f - (f_0 \pm \Delta f_{db}) + \Delta f_n = K_b(P_b - P_{b0}) \quad (11)$$

where Δf_n is frequency shift. The frequency shift is determined based on the control scenario. Later in this chapter, Δf_n will be defined. When the SOC level is in between SOC_{max1} and SOC_{min1} , the BESS operates on PS that is shown by the green line. There is no frequency shift applied in this scenario, thus Δf_n equals zero. This operation clearly aims to regulate its output power, in order to satisfy the power balance and keep the frequency within f_{max} and f_{min} . Assume the load demand P_{L1} is applied, the battery delivers P_{b1} while the generator delivers P_{d1} . If the load demand P_{L2} is applied, the BESS delivers $-P_{b2}$ while the generator delivers P_{d2} .

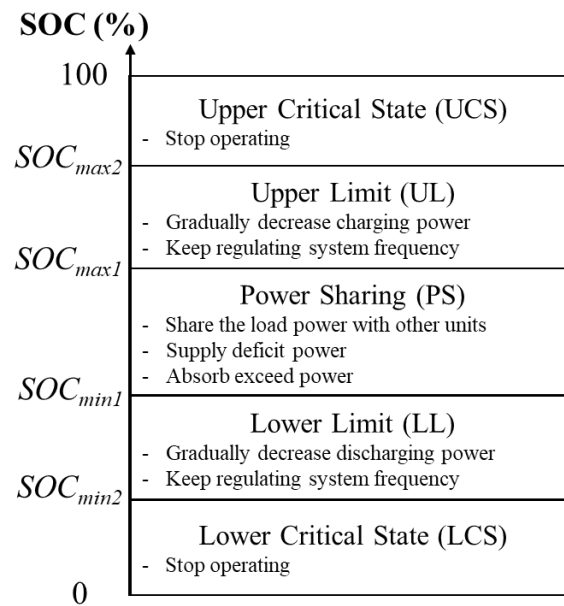
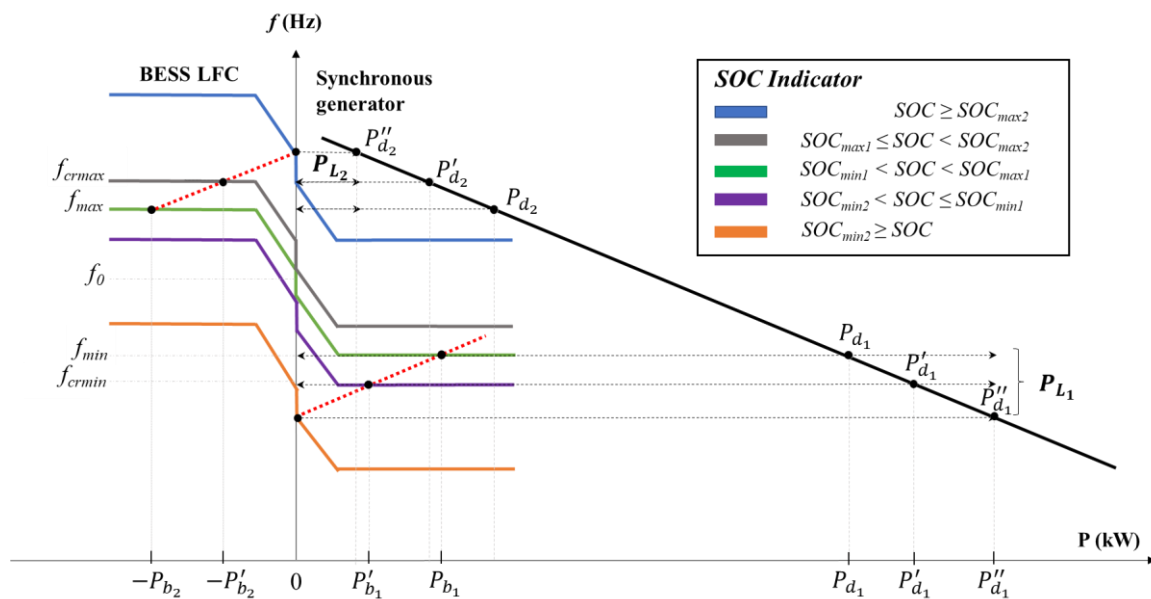


Figure 4. Proposed SOC control strategy.



By operating the battery at $SOC_{max1} \leq SOC < SOC_{max2}$, now the scenario changes to UL which illustrated by the grey line. This scenario allows the LFC (green line) curve to shift by Δf_n . It affects the nominal frequency of BESS to shift to $f_0 + \Delta f_n$ where Δf_n can be written as:

$$\Delta f_n = f_{\max} - f_{cr\max} \quad (12)$$

This operation shifts the maximum frequency to be f_{crmax} . By changing the nominal frequency, the operation point of BESS and generator are changed. Assume the load P_{L2} is applied while BESS charges its energy. In this case, the BESS delivers $-P_{b2}'$ and the generator output changes to P_{d2}' . This operation makes the BESS and the generator to establish a new operating point. By substituting Equation (12) to Equation (11), the curve can be expressed as:

$$f - (f_0 + \Delta f_{db}) + (f_{\max} - f_{cr\max}) = K_b(P_b - P_{b0}) \quad (13)$$

On the other hand, LL is activated when $SOC_{min2} < SOC \leq SOC_{min1}$ which illustrated by the purple line. This scenario allows the LFC (green line) curve to shift by Δf_n . It affects the nominal frequency of BESS shifting to $f_0 + \Delta f_n$ where Δf_n can be written as:

$$\Delta f_n = f_{\min} - f_{cr\min} \quad (14)$$

This operation allows the minimum frequency to be f_{crmin} . By changing its frequency limitation, the operation point of BESS and generator are changed. Assume the load demand P_{L1} is applied, the BESS delivers P_{b1}' while the generator delivers P_{d1}' . By substituting Equation (14) to Equation (11), the curve can be expressed as:

$$f - (f_0 - \Delta f_{db}) + (f_{\min} - f_{cr\min}) = K_b(P_b - P_{b0}) \quad (15)$$

The UCS is activated when the SOC level is over SOC_{max2} . In this scenario, the BESS stops its operation that brings the SOC remains at this level. Assuming that the load P_{L2} is applied, the BESS power becomes zero. It causes to meet all load demands by delivering P_{d2} . On the contrary, the LCS illustrated by the orange line actively operates if the SOC level is below SOC_{min2} . Assuming that the

load P_{L1} is applied, the BESS stops its operation. It causes the generator to meet all load demands by delivering P_{d1} .

In this control, the SOC level has a significant impact on the amount of battery output power, so the battery power always varies according to the SOC level. All those variations, from P_{b1} to zero or from P_{b2} to zero, can be correlated using a straight line illustrated by the dashed red line in Figure 5. This line describes the movement of BESS power in the presence of the droop reference shift due to SOC. The red line that shows the relation between frequency shift and power changes has an identical slope as the generator droop curve. Thus, the relation between frequency shift Δf and power changes ΔP written as:

$$\Delta P_{bn} = \Delta f_n \times \frac{1}{R} \quad (16)$$

where ΔP_{bn} is the BESS power changes, Δf_n is the frequency shift, and R is the generator droop gain. When the BESS enters the critical state, both UCS and LCS, the droop reference will shift according to the slope level of the generator droop described in equation (16). This shift causes the battery output to zero, so it can be written as:

$$0 - P_b = \Delta f_n \times \frac{1}{R} \quad (17)$$

Hence, it can be simplified into Equation (18).

$$-P_b \times R = \Delta f_n \quad (18)$$

Thus, by substituting Equation (18) into Equation (11), the Region 1 LFC can be written as:

$$f - (f_0 \pm \Delta f_{db}) + (-P_b \times R) = K_b(P_b - P_{b0}) \quad (19)$$

where it can be concluded that in every scenario, a frequency shift will be applied into the BESS LFC curve. Thus, the frequency shift Δf_n is written as in Equation (20).

$$\Delta f_n = \begin{cases} -P_b \times R; & SOC \geq SOC_{\max 2} \\ f_{\max} - f_{cr\max}; & SOC_{\max 1} \leq SOC < SOC_{\max 2} \\ 0; & SOC_{\min 1} < SOC < SOC_{\max 1} \\ f_{\min} - f_{cr\min}; & SOC_{\min 2} < SOC \leq SOC_{\min 1} \\ -P_b \times R; & SOC \leq SOC_{\min 2} \end{cases} \quad (20)$$

Every shift in Equation (20) is substituted into the LFC Equation (11) so that the reference shift applies in each region. Finally, the LFC curve that includes the SOC control is shown below:

$$P_b = \begin{cases} \frac{f - f_{\max} + \Delta f_n}{\left\{K_b \left(K_p + \frac{K_i}{s}\right)\right\}} + P_{b0}; & f \geq f_{\max} \\ \frac{f - (f_0 + \Delta f_{db}) + \Delta f_n}{K_b} + P_{b0}; & f_0 + \Delta f_{db} \leq f < f_{\max} \\ 0; & f_0 - \Delta f_{db} < f < f_0 + \Delta f_{db} \\ \frac{f - (f_0 - \Delta f_{db}) + \Delta f_n}{K_b} + P_{b0}; & f_{\min} < f \leq f_0 - \Delta f_{db} \\ \frac{f - f_{\min} + \Delta f_n}{\left\{K_b \left(K_p + \frac{K_i}{s}\right)\right\}} + P_{b0}; & f \leq f_{\min} \end{cases} \quad (21)$$

Equation (21) shows the completed LFC with SOC control. This control allows a load-sharing mechanism in BESS that monitors its SOC at the predetermined range.

A block diagram of proposed SOC control is shown in Figure 6. This control is distributed into four parts, from top to bottom, UCS, UL, LL, and LCS. The UCS and LCS scenarios use PI control ($K_{P_{soc}}$ and $K_{I_{soc}}$) so that the battery output can be maintained at zero, resulting in a frequency shift with zero BESS output power. Both the UL and LL scenarios only use simple mathematical operations because

the frequency shift has been defined to be f_{crmax} or f_{crmin} . The result of this block is a frequency shift that is passed on to the LFC block in Figure 3. The completed control block diagram contained LFC and SOC control is shown in Figure 7. This figure shows that the SOC condition at one time affects the BESS output power obtained from the LFC.

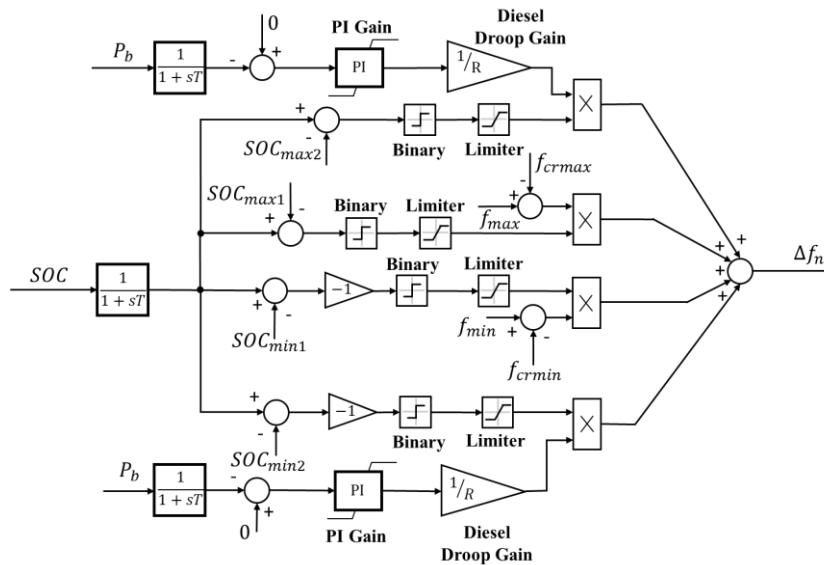


Figure 6. Proposed SOC control block diagram.

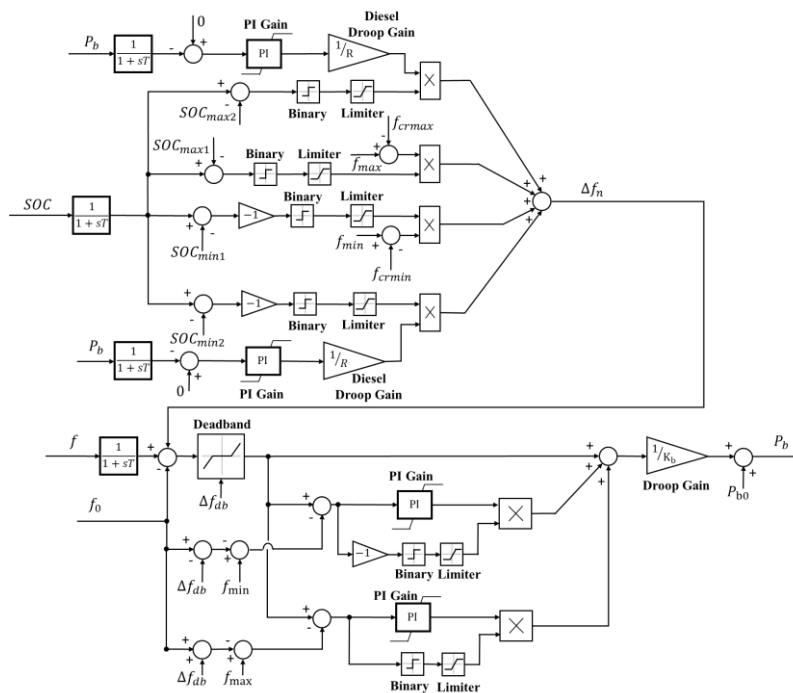


Figure 7. Proposed LFC with SOC control block diagram.

4. Attributes of the Test System

The performance of the proposed BESS control is examined on an islanded microgrid composed of a synchronous generator unit (diesel generator), consumer, PV, and BESS. Each unit is connected to the AC bus microgrid. The generator with a capacity of 390 kW and having a droop control on its governor acts as the system backbone. The installed PV is assumed to be able to deliver up to

200 kW. The installed BESS has a capacity of 2.5 Ah with the efficiency of PCS is 95%. The generator, PV, and BESS are network-integrated via a 0.4/13.2 kV step-up transformer. On the high voltage side, the transformer is connected to a 2 km long transmission line. At the end of the transmission line, a 13.2 kV/380 V step-down transformer connects the transmission to the load.

The system used in this study is illustrated in Figure 8. As the selected generator droop slope is 0.03 pu, the BESS droop slope is not determined based on the BESS capacity. However, the assumption used is that the selected BESS droop slope should be steeper than the generator. Therefore, the BESS is more sensitive to power variations compared to the generator.

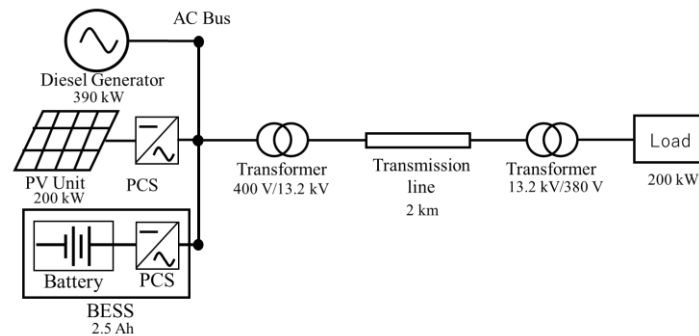


Figure 8. System Diagram.

The chosen battery capacity in this study is clearly small when compared to the real application. It is intended to facilitate the observation of the battery SOC variation in a short time. In this control implementation, the battery capacity mostly does not influence how much power will be delivered by the BESS. However, the battery capacity certainly affects the rate of change of the SOC. The implementation of a BESS with a small capacity has an impact on the time needed to reach a critical SOC (maximum or minimum) compared to a larger capacity. The smaller the BESS capacity, the faster the rate of change of SOC. Therefore, a relatively small capacity BESS is chosen so that the SOC could vary around 40–80% in a short time. Furthermore, the BESS control parameters used in this study are presented in Table 1. In this table the criteria control used for battery control are determined.

Table 1. Control parameter.

Description	Parameter	Value
Frequency operation limit	f_{max}	60.3 Hz
	f_{min}	59.7 Hz
Frequency deadband	Δf_{db}	0.1 Hz
Shifted frequency max limit	f_{crmax}	60.5 Hz
Shifted frequency min limit	f_{crmin}	59.5 Hz
Generator droop gain	R	0.03 pu
BESS droop gain	K_b	0.05 pu
LFC proportional gain	K_P	5
LFC integrator gain	K_I	0.02
SOC control proportional gain	K_{Psoc}	0.1
SOC Control integrator gain	K_{Isoc}	0.1
Initial SOC	$SOC_{initial}$	60.00%
	SOC_{max2}	75.00%
	SOC_{max1}	70.00%
BESS SOC level	SOC_{min1}	50.00%
	SOC_{min2}	45.00%

The study results are presented in two parts. The first part is the result of LFC verification. In this part, LFC is verified to be fully operational in all regions, from Region 1 to Region 3, by changing the PV power and load demands. The second part is the implementation of SOC control. In this section,

SOC control is verified to be fully operational in all control scenarios by changing the PV load and load demands. The results of the control implementation will be compared with and without the proposed control.

5. Results and Discussion

5.1. Load Frequency Control Result

The load frequency control is validated by applying load variations in the system. These variations will cause changes in the system operation. With the implementation of LFC, the frequency will be maintained within a prescribed range based on criteria control.

5.1.1. LFC Case 1—Load Increasing

In this case, the load is gradually increasing from 200 to 285 kW. First, the system is initiated at 60 Hz with the load demand of 200 kW, which puts BESS in standby mode. Figure 9a,b illustrates the active power and system frequency results, respectively.

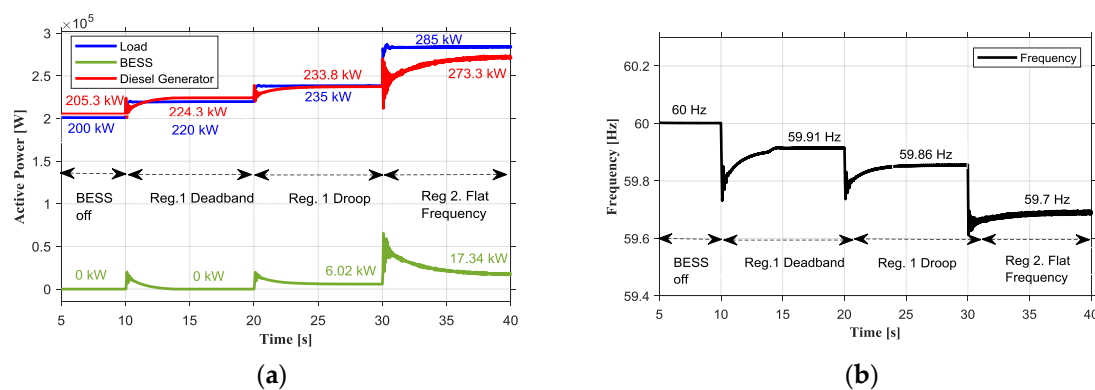


Figure 9. Result of LFC Case 1: (a) load, BESS, and diesel generator active power; (b) system frequency.

At $t = 10$ s, the load increases to 220 kW. It causes the frequency to drop as the generator tries to stabilize the system. The drop in the system frequency causes the battery to start operating and participating in the system. The participation of BESS creates a load sharing point that the BESS and generator must meet due to power imbalance. The point is reached at 59.91 Hz, the deadband area, that caused BESS in standby mode. At $t = 20$ s, the load increases to 235 kW. The same event is repeated wherein the BESS and generator have to reach the load sharing point reached at 59.86 Hz. Based on the BESS control design, now the battery works in Region 1 droop side. In this region, the BESS delivers 6.02 kW while the generator supplies 233.8 kW. Finally, the load increases to 285 kW that causes the frequency to become 59.7 Hz. In Region 2, the BESS continually suppresses the generator power at 273.3 kW by regulating its power to 17.34 kW. Despite another increase in load demand, the frequency will be maintained at 59.7 Hz as BESS continues to vary its output power. These results indicate that the LFC settles the generator output at the desired value by continuously regulating the BESS output power.

5.1.2. LFC Case 2—Load Decreasing

In this case, the load decreases gradually from 200 to 110 kW. The system is initiated at 60 Hz with the load demand of 200 kW, which puts BESS in standby mode. Figure 10a,b illustrate the active power of BESS, generator, and load and the system frequency, respectively. At $t = 10$ s, the load changes to 180 kW. This event causes the frequency to rise as the generator is trying to stabilize the system. The rise in the system frequency causes the battery to start operating and participating to the system. The participation of BESS creates a load sharing point that the BESS and generator must satisfy due to

the power imbalance. The point is reached at 60.09 Hz, the deadband area, puts the BESS in standby mode. At $t = 20$ s, the load decreases to 160 kW. The same event is repeated as the battery and the generator must find another load sharing point that reached at 60.15 Hz (Region 1 droop side). In this region, the generator delivers 172.5 kW and the battery delivers -6.75 kW. Finally, the load demand decreases to 110 kW that puts the frequency to become 60.3 Hz. In Region 3, the BESS continually suppresses the generator power at 138.6 kW by regulating its power at -22.74 kW. Despite another decrease in load demand, the frequency will be maintained at 60.3 Hz as BESS continues to regulate its output power.

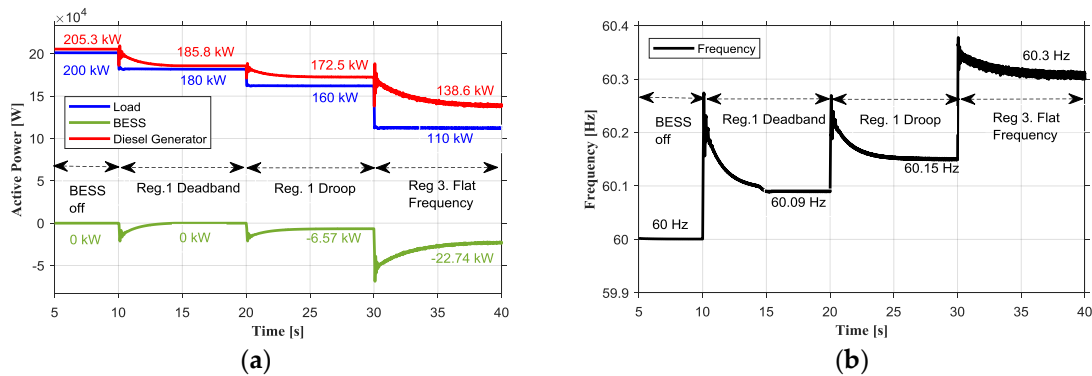


Figure 10. Result of LFC Case 2: (a) load, BESS, and diesel generator active power; (b) system frequency.

5.2. LFC with SOC Control

The implementation of the SOC control on BESS significantly changes the battery output power thus, the SOC remains within the specified range. In this section, variations in load and PV power are used to observe the performance of the proposed control.

5.2.1. SOC control Case 1—Load Increasing

In this case, the load increases from 200 to 290 kW. The system is initiated at 59.97 Hz and SOC at 60%. Figure 11a–c illustrates the BESS active power, system frequency, and the SOC, respectively. At $t = 10$ s, the load increases to 290 kW. It causes the system frequency drops from 60 Hz to around 59.6 Hz as the generator reaction. The reaction triggers the BESS to operate that is shown in Figure 11a,b. Once the battery participates to the system, both generator and BESS start finding the load sharing point to keep the power balance. The point is achieved at 59.7 Hz when the BESS supplies 29.2 kW. The power supplied by the BESS results in a decrease in SOC. It causes the SOC to decrease to SOC_{min1} as shown in Figure 11c. At $t = 20$ s, the SOC operation changes from PS to LL, where the minimum frequency limit changes to f_{crmin} , which puts the system frequency to 59.6 Hz. Changes in the minimum frequency limit unnecessarily make the frequency at f_{crmin} , yet the frequency still depends on the LFC curve. Now, the BESS power drops to 12.3 kW, which results in a less sharp drop in SOC compared to the PS scenario. With the same load demand, the declining SOC continues until it reaches SOC_{min2} . The SOC operation changes to LCS where BESS stops operating (returns to standby mode) and puts the SOC maintained at 45%. It causes the frequency to drop to 59.55 Hz, which comes from the governor system owned by the generator. In contrast, without implementing SOC control, the frequency is maintained at 59.7 Hz. However, a continuously decreasing SOC may cause the SOC to be outside its operating limits or the battery to be undercharged.

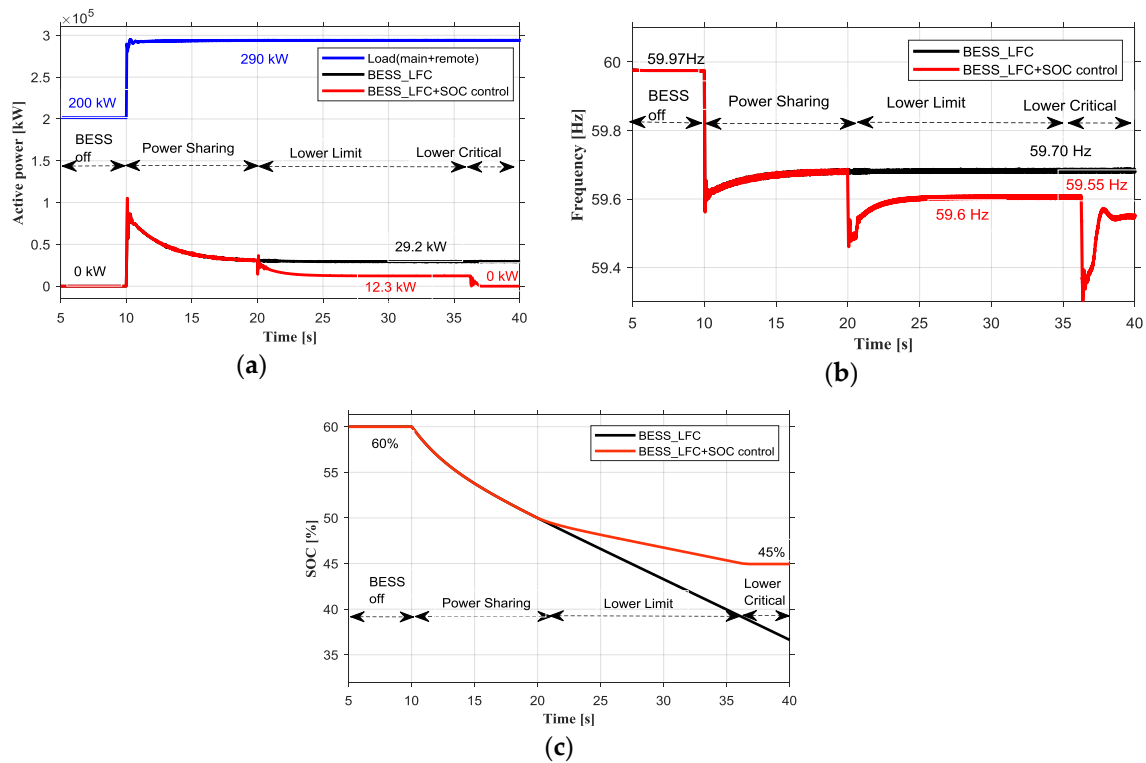


Figure 11. Result of LFC + SOC control Case 1: (a) load and BESS active power; (b) System frequency; (c) BESS SOC.

5.2.2. SOC Control Case 2—Load Decreasing

In this case, the load decreases from 200 to 100 kW. The system is initiated the same with the SOC control Case 1. Figure 12a–c illustrates the BESS active power, system frequency, and the BESS SOC, respectively. At $t = 10$ s, the load decreases to 100 kW. It causes the system frequency to rise to around 60.4 Hz as the system reaction. The reaction triggers the battery to operate, as shown in Figure 12a,b.

Once the battery participates in the system, both generator and battery start finding the load sharing point to keep the power balance. The point is achieved at 60.30 Hz when the battery delivers -27.2 kW. The power absorbed by BESS increases SOC. It causes the SOC to increase to SOC_{max1} as shown in Figure 12c. At $t = 20$ s, the SOC operation changes from PS to UL, where the maximum frequency limit changes to f_{crmax} , which puts the system frequency to 60.37 Hz. Changes in the maximum frequency limit unnecessarily make the frequency at f_{crmax} , yet the frequency still depends on the LFC curve. Now, the BESS charging power has dropped to -9.82 kW, which results in a less sharp rise in SOC compared to the PS scenario. With the same load demand, the incline in SOC continues until it reaches SOC_{max2} . The SOC operation changes to UCS, where BESS stops operating (returns to standby mode) and puts the SOC maintained at 75%. It causes the frequency to rise to 60.41 Hz, which comes from the governor's system owned by the generator. In contrast, without implementing SOC control, the frequency is maintained at 60.30 Hz. However, a continuously increasing SOC may cause the SOC to be outside its operating limits or the battery to be overcharged.

5.2.3. SOC Control Case 3—PV Power Increasing

In this case, the load is maintained at 200 kW, while the PV power increases from 100 to 200 kW. The system is initiated at 59.97 Hz and SOC at 60%. Figure 13a–c illustrate the BESS active power, system frequency, and the BESS SOC, respectively. At $t = 10$ s, the PV increases to 200 kW. It causes the system frequency to rise to around 60.4 Hz as the system reaction. The reaction triggers the battery to operate shown in Figure 13a,b.

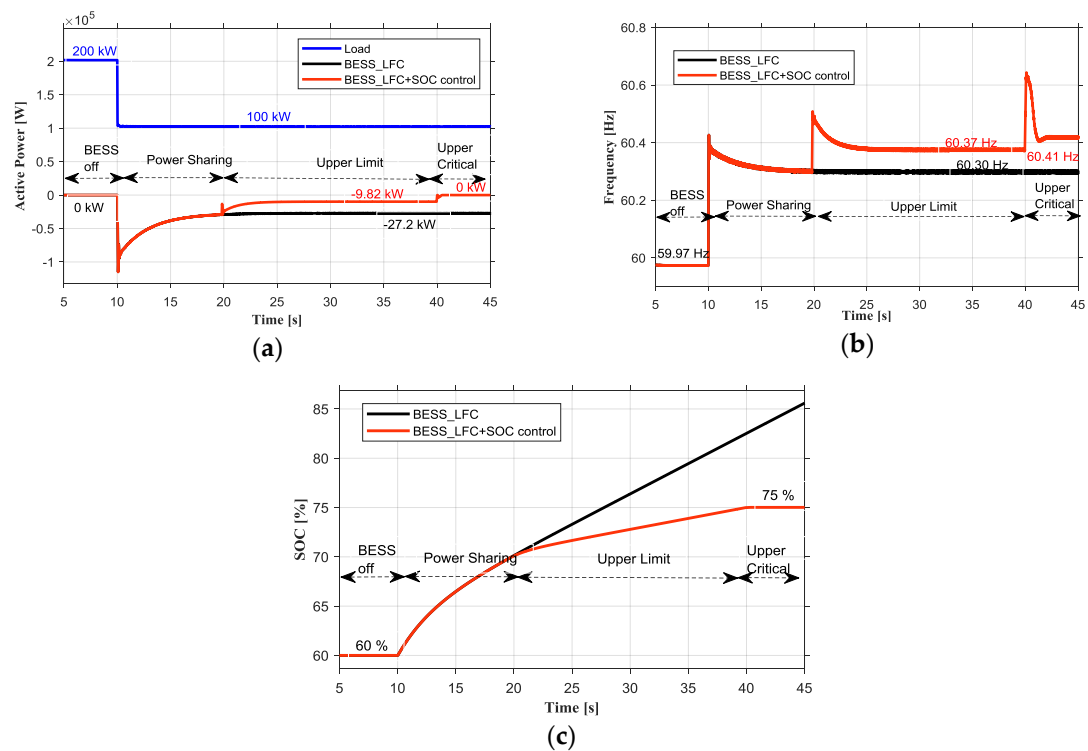


Figure 12. Result of LFC + SOC control Case 2: (a) load and BESS active power; (b) system frequency; (c) BESS SOC.

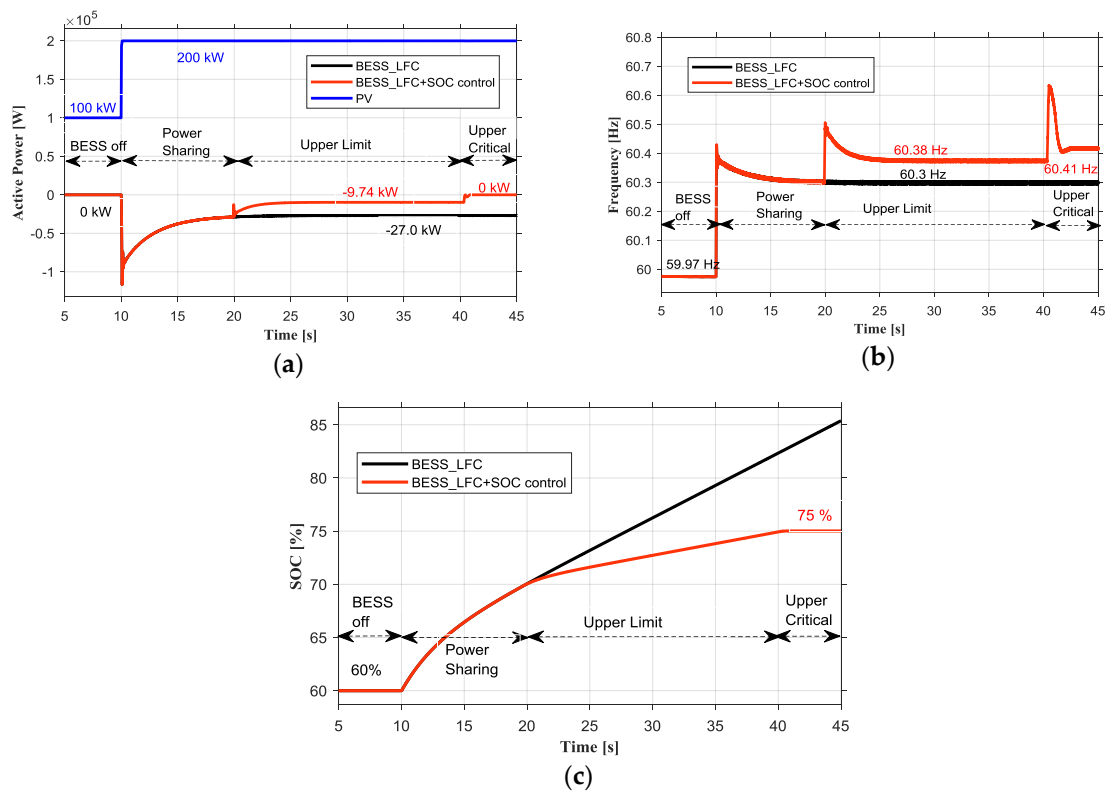


Figure 13. Result of LFC + SOC control Case 3: (a) PV and BESS active power; (b) system frequency; (c) BESS SOC.

Once the battery participates in the system, both generator and battery start finding the load sharing point to keep the power balance. The point is achieved at 60.30 Hz when the battery delivers -27.0 kW. The power absorbed by BESS increases SOC. It causes the SOC to increase to SOC_{max1} as shown in Figure 13c. At $t = 20$ s, the SOC operation changes from PS to UL, where the maximum frequency limit changes to f_{crmax} , which puts the system frequency to 60.38 Hz. Changes in the maximum frequency limit unnecessarily make the frequency at f_{crmax} , yet the frequency still depends on the LFC curve. Now, the BESS charging power has dropped to -9.74 kW, which results in a less intense rise in SOC compared to the PS scenario. With the same load demand, the incline in SOC continues until it reaches SOC_{max2} . The SOC operation changes to UCS, where BESS stops operating (returns to standby mode) and puts the SOC maintained at 75%. It causes the frequency to rise to 60.41 Hz, which comes from the governor's system owned by the generator. In contrast, without implementing SOC control, the frequency was maintained at 60.30 Hz. However, a continuously increasing SOC may cause the SOC to be outside its operating limits or the battery to be overcharged.

5.2.4. SOC Control Case 4—PV Power Decreasing

In this case, the load is maintained at 200 kW, while the PV power decreases from 100 to 0 kW. The system is initiated the same with the SOC control Case 3. Figure 14a–c illustrate the BESS active power, system frequency, and the BESS SOC, respectively. At $t = 10$ s, the PV decreases to 0 kW. It causes the system frequency to drop to around 59.6 Hz as the system reaction. The reaction triggers the battery to operate, as shown in Figure 14a,b.

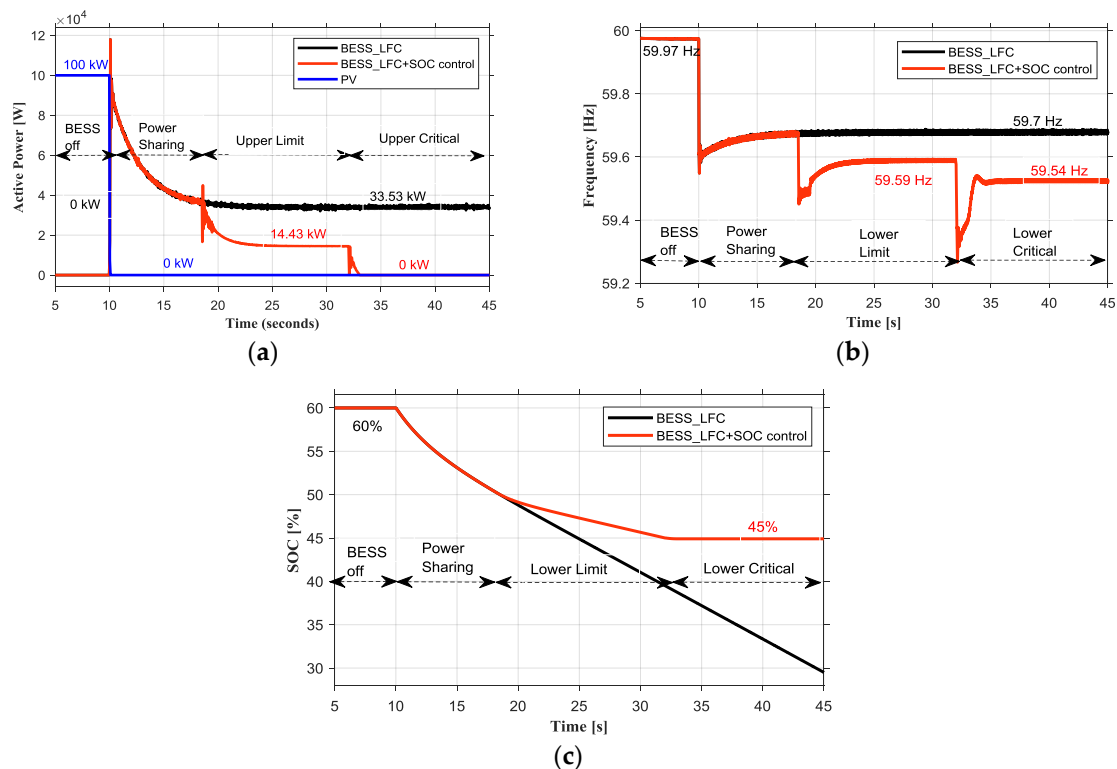


Figure 14. Result of LFC + SOC control Case 4: (a) photovoltaic (PV) and BESS active power; (b) system frequency; (c) BESS SOC.

Once the battery participates in the system, both generator and battery start finding the load sharing point to keep the power balance. The point is achieved at 59.7 Hz when the battery delivers 33.53 kW. The power supplied by BESS decreases SOC. It causes the SOC to decrease to SOC_{min1} as shown in Figure 14c. At $t = 20$ s, the SOC operation changes from PS to LL, where the maximum frequency limit changes to f_{crmin} , which puts the system frequency to 59.59 Hz. Changes in the

minimum frequency limit unnecessarily make the frequency at f_{crmin} , yet the frequency still depends on the LFC curve. Now, the BESS power has dropped to 14.43 kW, which results in a less intense drop in SOC compared to the PS scenario. With the same load demand, the decline in SOC continues until it reaches SOC_{min2} . The SOC operation changes to LCS, where BESS stops operating (returns to standby mode) and puts the SOC maintained at 45%. It causes the frequency to drop to 59.54 Hz, which comes from the governor's system owned by the generator. In contrast, without implementing SOC control, the frequency was maintained at 59.70 Hz. However, a continuously decreasing SOC may cause the SOC to be outside its operating limits or the battery to be undercharged.

6. Conclusions

In this article, a SOC control integrated with BESS LFC has been proposed for an islanded microgrid. The proposed control has five control scenarios, which are achieved by applying the LFC reference shift method. These scenarios are upper critical state (UCS), upper limit (UL), power sharing (PS), lower limit (LL), and lower critical state (LCS). The scenarios are separated based on predetermined SOC level, named SOC_{max2} , SOC_{max1} , SOC_{min1} , and SOC_{min2} , where the maximum and minimum values of the LFC curve can shift to f_{crmax} , f_{crmin} , or to the point where the battery stops operating.

Based on the simulation results shown in this article, the proposed control provides SOC and frequency regulation, while sharing power proportionally to the generator. The rate of change of SOC is proportional to the magnitude of the BESS output power. The SOC control allows switching control scenarios by shifting the LFC frequency reference. It causes the BESS output power to change based on the control scenario. Thus, the SOC remains within the predetermined range.

By applying $SOC_{max2} = 75\%$, $SOC_{max1} = 70\%$, $SOC_{min1} = 50\%$, and $SOC_{min2} = 45\%$ as criteria control, SOC BESS can be maintained at 45–75% when the system is suffering from changes in load and PV power. When the SOC control works, the system frequency is maintained by applying LFC to BESS, which applies multiple region control.

Although the proposed control carries technical advantages, it does not optimize microgrid operation from a cost of BESS life cycle point of view. Economic analysis with the application of the proposed control remains an open scientific problem. Moreover, the analysis carried out is achieved based on one generator and one BESS only. Further investigations with complex systems need to be carried out, such as multi-machines and variations of renewable energy sources.

Author Contributions: Conceptualization, S.S.; methodology, S.S. and Y.H.; software, S.S. and Y.H.; validation, S.S., Y.H., V.B. and G.F.; formal analysis, S.S. and Y.H.; investigation, S.S.; resources, V.B. and G.F.; data curation, S.S. and Y.H.; writing—original draft preparation, S.S. and Y.H.; writing—review and editing, S.S., Y.H., V.B. and G.F.; visualization, S.S.; supervision, V.B. and G.F.; project administration, G.F.; funding acquisition, V.B. All authors have read and agreed to the published version of the manuscript.

Funding: This research was supported by Nippon Koei Co., Ltd.

Conflicts of Interest: The authors declare no conflict of interest.

References

1. Mercier, P.; Cherkaoui, R.; Oudalov, A. Optimizing a Battery Energy Storage System for Frequency Control Application in an Isolated Power System. *IEEE Trans. Power Syst.* **2009**, *24*, 1469–1477. [\[CrossRef\]](#)
2. Llaría, A.; Cúrea, O.; Jiménez, J.; Camblong, H. Survey on microgrids: Unplanned islanding and related inverter control techniques. *Renew. Energy* **2011**, *36*, 2052–2061. [\[CrossRef\]](#)
3. Tan, X.; Li, Q.; Wang, H. Advances and trends of energy storage technology in Microgrid. *Int. J. Electr. Power Energy Syst.* **2013**, *44*, 179–191. [\[CrossRef\]](#)
4. Aghamohammadi, M.R.; Abdolahinia, H. A new approach for optimal sizing of battery energy storage system for primary frequency control of islanded Microgrid. *Int. J. Electr. Power Energy Syst.* **2014**, *54*, 325–333. [\[CrossRef\]](#)

5. Datta, U.; Kalam, A.; Shi, J. Battery Energy Storage System Control for Mitigating PV Penetration Impact on Primary Frequency Control and State-of-Charge Recovery. *IEEE Trans. Sustain. Energy* **2020**, *11*, 746–757. [\[CrossRef\]](#)
6. Ocon, J.D.; Bertheau, P. Energy Transition from Diesel-based to Solar Photovoltaics-Battery-Diesel Hybrid System-based Island Grids in the Philippines—Techno-Economic Potential and Policy Implication on Missionary Electrification. *J. Sustain. Dev. Energy Water Environ. Syst.* **2019**, *7*, 139–154. [\[CrossRef\]](#)
7. Eftekharnejad, S.; Vittal, V.; Heydt, G.T.; Keel, B.; Loehr, J. Small Signal Stability Assessment of Power Systems With Increased Penetration of Photovoltaic Generation: A Case Study. *IEEE Trans. Sustain. Energy* **2013**, *4*, 960–967. [\[CrossRef\]](#)
8. You, S.; Kou, G.; Liu, Y.; Zhang, X.; Cui, Y.; Till, M.J.; Yao, W.; Liu, Y. Impact of High PV Penetration on the Inter-Area Oscillations in the U.S. Eastern Interconnection. *IEEE Access* **2017**, *5*, 4361–4369. [\[CrossRef\]](#)
9. Liu, Y.; Wang, X. Research on Frequency Control of Islanded Microgrid with Multiple Distributed Power Sources. *Processes* **2020**, *8*, 193. [\[CrossRef\]](#)
10. Li, T.; Wen, B.; Wang, H. A Self-Adaptive Damping Control Strategy of Virtual Synchronous Generator to Improve Frequency Stability. *Processes* **2020**, *8*, 291. [\[CrossRef\]](#)
11. Tucci, M.; Ferrari-Trecate, G. A scalable, line-independent control design algorithm for voltage and frequency stabilization in AC islanded microgrids. *Automatica* **2020**, *111*, 108577. [\[CrossRef\]](#)
12. Parvizmosaed, M.; Zhuang, W. Enhanced Active and Reactive Power Sharing in Islanded Microgrids. *IEEE Syst. J.* **2020**, 1–12. [\[CrossRef\]](#)
13. Aminzadeh, S.; Tarafdar Hagh, M.; Seyedi, H. Reactive power management for microgrid frequency control. *Int. J. Electr. Power Energy Syst.* **2020**, *120*, 105959. [\[CrossRef\]](#)
14. Pinthurat, W.; Hredzak, B. Decentralized Frequency Control of Battery Energy Storage Systems Distributed in Isolated Microgrid. *Energies* **2020**, *13*, 3026. [\[CrossRef\]](#)
15. Stroe, D.-I.; Knap, V.; Swierczynski, M.; Stroe, A.-I.; Teodorescu, R. Operation of a Grid-Connected Lithium-Ion Battery Energy Storage System for Primary Frequency Regulation: A Battery Lifetime Perspective. *IEEE Trans. Ind. Appl.* **2017**, *53*, 430–438. [\[CrossRef\]](#)
16. Jo, H.; Choi, J.; Agyeaman, K.A.; Han, S. Development of frequency control performance evaluation criteria of BESS for ancillary service: A case study of frequency regulation by KEPCO. In Proceedings of the 2017 IEEE Innovative Smart Grid Technologies-Asia (ISGT-Asia), Auckland, New Zealand, 4–7 December 2017; pp. 1–5.
17. Li, D.; Wu, Z.; Zhao, B.; Zhang, L. An Improved Droop Control for Balancing State of Charge of Battery Energy Storage Systems in AC Microgrid. *IEEE Access* **2020**, *8*, 71917–71929. [\[CrossRef\]](#)
18. Shim, J.W.; Verbic, G.; Zhang, N.; Hur, K. Harmonious integration of faster-acting energy storage systems into frequency control reserves in power grid with high renewable generation. *IEEE Trans. Power Syst.* **2018**, *33*, 6193–6205. [\[CrossRef\]](#)
19. Tan, Z.; Li, X.; He, L.; Li, Y.; Huang, J. Primary frequency control with BESS considering adaptive SoC recovery. *Int. J. Electr. Power Energy Syst.* **2020**, *117*, 105588. [\[CrossRef\]](#)
20. Shim, J.W.; Verbic, G.; Kim, H.; Hur, K. On Droop Control of Energy-Constrained Battery Energy Storage Systems for Grid Frequency Regulation. *IEEE Access* **2019**, *7*, 166353–166364. [\[CrossRef\]](#)
21. IEEE. *Guide for Design, Operation, and Integration of Distributed Resource Island Systems with Electric Power Systems*; IEEE: Piscataway, NJ, USA, 2011.
22. Datta, U.; Kalam, A.; Shi, J. Battery Energy Storage System for Aggregated Inertia-Droop Control and a Novel Frequency Dependent State-of-Charge Recovery. *Energies* **2020**, *13*, 2003. [\[CrossRef\]](#)
23. Stavrakakis, G.S.; Kariniotakis, G.N. A general simulation algorithm for the accurate assessment of isolated diesel-wind turbines systems interaction. I. A general multimachine power system model. *IEEE Trans. Energy Convers.* **1995**, *10*, 577–583. [\[CrossRef\]](#)
24. Yeager, K.E.; Willis, J.R. Modeling of emergency diesel generators in an 800 megawatt nuclear power plant. *IEEE Trans. Energy Convers.* **1993**, *8*, 433–441. [\[CrossRef\]](#)
25. NEPLAN AG Turbine-Governor Models. Available online: https://www.neplan.ch/wp-content/uploads/2015/08/Nep_TURBINES_GOV.pdf (accessed on 14 March 2020).
26. Woodward Speed Droop and Power Generation. 1991. Available online: <http://www.woodward.com/WorkArea/DownloadAsset.aspx?id=2147483661> (accessed on 15 March 2020).
27. Divya, K.C.; Østergaard, J. Battery energy storage technology for power systems—An overview. *Electr. Power Syst. Res.* **2009**, *79*, 511–520. [\[CrossRef\]](#)

28. Hill, C.A.; Such, M.C.; Chen, D.; Gonzalez, J.; Grady, W.M.K. Battery energy storage for enabling integration of distributed solar power generation. *IEEE Trans. Smart Grid* **2012**, *3*, 850–857. [[CrossRef](#)]
29. Mantar Gundogdu, B.; Nejad, S.; Gladwin, D.T.; Foster, M.P.; Stone, D.A. A Battery Energy Management Strategy for U.K. Enhanced Frequency Response and Triad Avoidance. *IEEE Trans. Ind. Electron.* **2018**, *65*, 9509–9517. [[CrossRef](#)]
30. Sebastián, R. Application of a battery energy storage for frequency regulation and peak shaving in a wind diesel power system. *IET Gener. Transm. Distrib.* **2016**, *10*, 764–770. [[CrossRef](#)]
31. Xu, Y.; Li, C.; Wang, Z.; Zhang, N.; Peng, B. Load Frequency Control of a Novel Renewable Energy Integrated Micro-Grid Containing Pumped Hydropower Energy Storage. *IEEE Access* **2018**, *6*, 29067–29077. [[CrossRef](#)]
32. Ahn, S.-J.; Park, J.-W.; Chung, I.-Y.; Moon, S.-I.; Kang, S.-H.; Nam, S.-R. Power-Sharing Method of Multiple Distributed Generators Considering Control Modes and Configurations of a Microgrid. *IEEE Trans. Power Deliv.* **2010**, *25*, 2007–2016. [[CrossRef](#)]
33. Senjyu, T.; Kikunaga, Y.; Yona, A.; Funabashi, T. Study on Optimum Capacity of Battery Energy Storage System for Wind Power Generator. *IEE J. Trans. Power Energy* **2008**, *128*, 321–327. [[CrossRef](#)]



© 2020 by the authors. Licensee MDPI, Basel, Switzerland. This article is an open access article distributed under the terms and conditions of the Creative Commons Attribution (CC BY) license (<http://creativecommons.org/licenses/by/4.0/>).